Geophys. J. Int. (2006) **167,** 1363–1372 doi: 10.1111/j.1365-246X.2006.03139.x

Radiative transfer theory for estimation of the seismic moment

C. Sens-Schönfelder and U. Wegler

Universität Leipzig, Talstr. 35, 04103 *Leipzig, Germany.*
E-mail: sens-schoenfelder@uni-leipzig.de

Accepted 2006 July 12. Received 2006 June 6; in original form 2006 February 22

SUMMARY

We propose a new technique to obtain source spectra and seismic moments of regional earthquakes from envelopes of seismic coda. As compared to existing methods, our approach is based on a physical model of the scattering process that produces the seismic coda. This allows the direct estimation of source parameters, without the necessity to fix proportionality coefficients with reference events. We see an appreciable advantage because the method is independent of the output from other techniques, such as reference events provided by moment inversions. The main component of our method is a joint inversion of the seismic records for source and site parameters, as well as for medium parameters assuming isotropic sources and isotropic, acoustic scattering in a half-space.

The method is tested with recordings of 11 earthquakes ($4 \leq M_l \leq 6$) by the German Regional Seismic Network at epicentral distances less than 1000 km. We invert the traces in eight frequency bands between 0.2 and 24 Hz and demonstrate that our estimates of the seismic moment are in good agreement with values obtained in independent studies using waveform inversion techniques. In fact our estimates of the seismic moment are better than approximations obtained from local magnitudes using empirical relations specifically derived for the region under study. The parameters that describe the scattering medium are mean free path that we found to average around 690 km and the intrinsic quality factor for which we obtain ${}^{I}Q = 500$ below 3 Hz.

Key words: coda, radiative transfer theory, scattering, seismic moment.

1 INTRODUCTION

Since it has been recognized for some time that amplitudes of regional coda are proportional to source excitation, attempts to extract information about the seismic source from the coda have a long history. Aki & Chouet (1975) were the first to study source spectra with coda waves. Due to the available instruments they obtained source spectra above 3 Hz. A correction for attenuation is necessary that involves an empirical quality factor describing both intrinsic and scattering attenuation. The measurements are made relative to each other and have to be adjusted to reference events. Mayeda & Walter (1996) used 2-D multiple scattering to approximate coda envelopes and to measure coda amplitudes. Above 0.2 Hz, additional empirical distance corrections were introduced. Mayeda & Walter (1996) proposed that the influence of body wave scattering, which is not described by their 2-D scattering model, required this empirical modification. They transformed the frequency resolved coda amplitudes to moment-rate spectra using reference events. Mayeda *et al.* (2003) extended this empirical approach and ended up with 12 free parameters describing the coda envelopes. Mayeda *et al.* (2003) tested the method and applied it to the Dead Sea Rift. Morasca *et al.* (2005) used it to analyse energy-moment scaling in the western Alps. The approach of Mayeda *et al.* (2003) and Morasca *et al.* (2005) is completely empirical and has no connection to the physics of the scattering process. Dewberry & Crosson (1995) used the single-scattering model in a detailed analysis of seismic source spectra of 78 northwestern US earthquakes. They also provided coda Q and site amplification estimates.

All these studies share the fact that they need reference events with known source spectra to fix proportionality coefficients to obtain absolute values for the source spectra. In contrast, the approach presented here is independent of external information because the physical model of the scattering provides a direct relation between the amplitude of the coda and the source excitation without any proportionality coefficient. This direct relation was previously used by Nakahara *et al.* (1998). Based on theoretical developments by Sato *et al.* (1997), they presented an approach to study the source process of large earthquakes in great detail. Nakahara *et al.* (1998) used a model of multiple isotropic acoustic scattering to invert for the spatial distribution of non-isotropic high-frequency energy radiation on the fault plane. In this method, medium parameters are taken from studies that belong to another branch of coda investigations.

The aforementioned studies focus on the properties of the propagation medium rather than on the source and aim to separate the effects of intrinsic and scattering attenuation to characterize the small-scale heterogeneities and the dissipation of energy. There

are, for example, several studies (Fehler *et al.* 1992; Mayeda *et al.* 1992; Bianco *et al.* 2002) applying the multiple lapse time window analysis (MLTWA) as developed by Hoshiba *et al.* (1991). MLTWA is based on multiple isotropic acoustic scattering and uses ratios of energy integrated in three consecutive time windows to separate intrinsic and scattering attenuation. An improvement to the geometrical setting is due to Margerin *et al.* (1998), who model energy propagation in a layer above a half-space. Lacombe *et al.* (2003) use a similar model consisting of a scattering layer overlaying a transparent half-space to characterize the attenuation properties of L_g waves. All these studies apply coda-normalization (Aki 1980) to correct for unwanted effects of the source and site amplifications. Coda-normalization, however, fails for small events with a shorter coda, because the coda can be dominated by random seismic noise before the requirement of homogeneous distribution of energy in space is fulfilled. In the present study, we overcome this disadvantage by including source excitation and site amplification directly in the inversion process.

We present an approach to estimate the source spectrum by jointly inverting the seismic record for medium parameters and source/site effects. The merit of this integrated approach is that

(i) it is independent of external information such as the source spectrum of reference events because we utilize a physical model of the scattering process for which we obtain the parameters in the inversion. This model provides a direct relation between coda amplitude and source excitation.

(ii) it is applicable for smaller events because the source excitation and the site amplification factors are estimated within the inversion, thus no coda-normalization is needed.

The paper is organized as follows. We describe the modelling of seismogram envelopes in Section 2 and introduce the data selection and the study area in Section 3. We describe the inversion scheme in Section 4 and show results of the inversion in Section 5.

2 ENVELOPE MODELLING

Envelopes are modelled using radiative transfer theory. Scattering of waves in 3-D space is governed by the radiative transfer or Boltzmann equation (Margerin *et al.* 1998). Here we restrict ourselves to isotropic scattering of *S*-waves in a half-space with an isotropic source. In full-space the effective energy density Green's function $G(t, \mathbf{r})$ is given by the following integral equation

$$G(t,\mathbf{r}) = F(t,\mathbf{r}) + v_0 g_0 \int_{-\infty}^{\infty}\int_V F(t-t',\mathbf{r}-\mathbf{r}')G(t',\mathbf{r}')\,dt'\,d\mathbf{r}', \tag{1}$$

(Sato & Fehler 1998, p. 175).

$$F(t,\mathbf{r}) = \frac{1}{4\pi v_0 r^2} H(t)\delta(t-r/v_0)e^{-v_0 g_o t}, \tag{2}$$

is the Green's function for the coherent wave energy. Here v_0 and g_0 denote average velocity of *S*-waves and total scattering coefficient, respectively. $r = |\mathbf{r}|$ is the source receiver distance and H is the Heaviside step function. The exact solution of eq. (1) involves a 2-D Fourier transform (Zeng *et al.* 1991; Sato & Fehler 1998, p. 177).

To speed up the inversion we use an analytic approximation to the solution of 1 obtained by Paasschens (1997) by interpolating between the explicit solutions of the Boltzmann equation in 2-D and 4-D. The solution of Paasschens (1997) reads

$$G(t,r) \simeq \frac{e^{-v_0 t g_0}}{4\pi r^2}\delta(r-v_0 t) + \frac{\left(1-r^2/\left(v_0^2 t^2\right)\right)^{1/8}}{\left(4\pi\, v_0 t/(3g_0)\right)^{3/2}} \times e^{-v_0 t g_0} K\left(v_0 t g_0\left[1-\frac{r^2}{v_0^2 t^2}\right]^{3/4}\right) H(v_0 t - r), \tag{3}$$

where $K(x) \simeq e^x\sqrt{1+2.026/x}$. Recently this interpolation was used by Abubakirov (2005) in a MLTWA. It is a good approximation to the solution of eq. (1) given by Zeng *et al.* (1991). The deviation from the exact solution is below 5 per cent where larger deviations occur in the tail of the direct wave. The accuracy of the approximation for the direct wave and its tail is reasonable in our context because we will only use an average value in a short time window following the direct wave. This time window is largely dominated by the energy of the unscattered wave which is correctly described in eq. (3).

The boundary condition for radiative transfer in a half-space is zero vertical energy flux at the surface. Assuming total reflection, we account for this condition by introducing a mirror source above the surface for which the energy density Green's function is $G(t, r^+)$, with r^+ being the distance between receiver and mirror source. At the surface the upward flux of the real source equals the downward flux of the mirror source, thereby satisfying the boundary condition. The energy density Green's function of the half-space is thus $G_h(t, \mathbf{x}) = G(t, r) + G(t, r^+)$. In the following we assume that the receiver is at the surface where $r = r^+$. In this case $G_h(t, \mathbf{x}) = 2G(t, r)$ (*cf.* Wegler 2004). With this treatment we only consider the boundary condition for energy transfer. Specific effects arising from boundary conditions of the wave equation like mode conversions, surface waves and angle-dependent reflection coefficients are not accounted for.

The energy density for an arbitrary source can be obtained by convolution with the source function. In our analysis we assume a source function of the form $W\delta(\mathbf{r})\delta(t)$ where W is the spectral source energy in J/Hz. Intrinsic absorption can be accounted for with an additional time-dependent factor e^{-bt} with the intrinsic absorption parameter b. Finally we obtain

$$E_{\mathrm{mod}}(t,\mathbf{x}) = W R_i G_h(t,\mathbf{x}) e^{-bt}, \tag{4}$$

$$= 2W R_i G(t,r) e^{-bt}, \tag{5}$$

for the energy density $E_{\mathrm{mod}}(t, r)$ of our half-space model at time t and distance r from the source of energy W. R_i is the site response at station i.

3 DATA AND REGIONAL SETTING

Data for this study was recorded by the German Regional Seismic Network (GRSN), the Gräfenberg array (GRF) and the reference station of the GERESS-array. The stations are equipped with STS-2 or STS-1 (GRF stations) broad-band seismometers and traces are sampled at 80 Hz. Refer to Korn (2002) for a detailed discussion from the GRSN. For this work we use data of 25 different stations (Fig. 1).

As sources we use local and regional events from Germany and adjacent areas in the period from the installation of the GRSN in 1991 until 2004 December. We choose events with local magnitudes estimated by the German Central Seismological Observatory (SZGRF) larger or equal to 4. To reduce scatter in the estimates of our parameters we exclude events from the Alps because of the

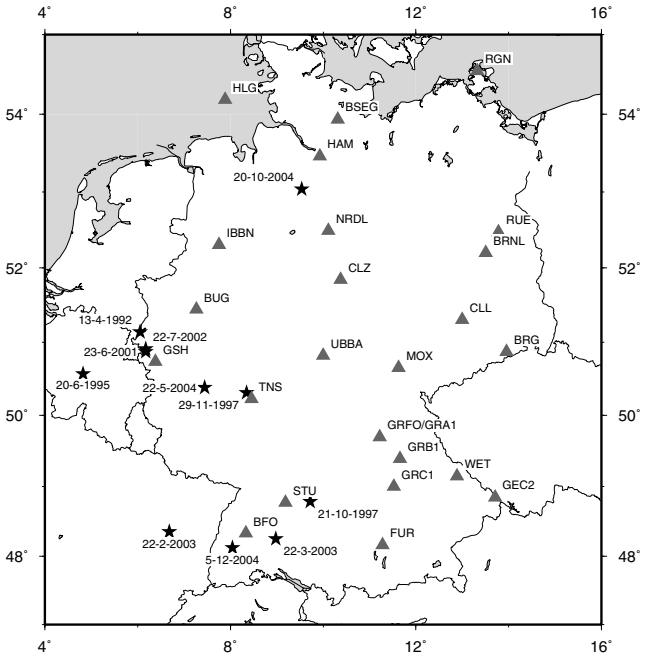

Figure 1. Map of Germany and neighbouring countries. Grey triangles: broad-band stations of the German Regional Seismic Network, the Gräfenberg array and the GERESS station GEC2 (station codes are added); black stars: earthquakes used in this study (dates of occurrence are added).

differences in the geological conditions. One event that occurred on 1994 October 18 in the North Sea is excluded because we observed suspicious differences in the arrival times, perhaps due to location errors or an unsuitable velocity model. In the end we use 11 earthquakes (Fig. 1) and more than 100 three-component broad-band records. Locations, magnitudes and depths as provided by the SZGRF are listed in Table 1. With the possible exception of the Roermond 1992 earthquake, where depths even below 20 km have been estimated (Korn 2002), the events occurred in the upper crust. The last three columns of Table 1 contain seismic moments estimated by waveform modelling and the method presented here. They will be discussed later.

Preparation of data involves filtering of the seismograms in eight frequency bands centred at 0.1875, 0.375, 0.75, 1.5, 3.0, 6.0, 12.0 and 24.0 Hz with a narrow normalized Gaussian filter. Choosing the filter such that $\int_{-\infty}^{\infty} |B(f)|^2\, df = 1$ where $B(f)$ is the frequency response, ensures that the spectral energy density is preserved in the filter process (Wegler *et al.* 2006) . Envelope sections are selected according to the following criteria:

(i) S/N—ratio greater than 4
(ii) No obvious disturbances, for example, aftershocks (checked manually)
(iii) Hypocentral distance greater than 60 km.

The hypocentral distance range is limited to distances greater than 60 km because we use a simple half-space velocity model, with a mean shear wave speed $v_0 = 3.5$ km s^{-1}, which is inappropriate for shorter distances.

We obtain the observed energy density $E_{\rm obs}(t, r)$, that is, the seismogram envelopes, from the bandpassed velocity seismogram $\dot{u}(t, r)$ using

$$E_{\rm obs}(t, r) = \frac{\rho_0}{2} \frac{\dot{u}^2(t, r) + \mathcal{H}^2(\dot{u}(t, r))}{2}. \quad (6)$$

Here ρ_0 is the mean density of the medium and $\mathcal{H}$ denotes the Hilbert transform. We use $\rho_0 = 2700$ kg m^{-3} throughout this study.

4 INVERSION

In the inversion scheme we estimate values for the parameters g_0, b, W and R_i that minimize the misfit function

$$\epsilon = \sum_{i=1}^{N} \sum_{j=\mathrm{start}_i}^{\mathrm{end}_i} \left[\log\left(\frac{E_{\rm obs}(t_j, r_i)}{E_{\rm mod}(t_j, r_i)} \right) \right]^2. \quad (7)$$

Here N denotes the number of stations. start$_i$ and end$_i$ correspond to the indices of the first and the last sample in the 'coda' time window (Fig. 2) at the ith station. The 'coda' time window starts after twice the S-wave traveltime and ends when the S/N drops below 4. We simultaneously invert all available traces of a certain event in one frequency band jointly for g_0, b, W and R_i. The inversion scheme is a combination of a 1-D grid search for g_0 and a linear inversion for the remaining parameters. Fig. 2 illustrates the constraints of this process which works in the following five steps.

(i) We pick a value of g_0 (a range of g_0 is probed in a grid search) and calculate the energy density Green's functions $G(t, r_i)$ for all stations i, using the approximation in eq. (3).

Table 1. List of earthquakes used in this study. Source time, location, depth and local magnitudes are provided by the German Central Seismological Observatory. Seismic moments estimated by modelling waveforms are listed in column 6 with respective references in column 7. The last column lists seismic moments estimated in the present study.

Date	Time	Location	Ml	Depth	$M_0^{\rm wm}$ in N m (waveform modelling)	Reference	$M_0^{\rm coda}$ in N m (this study)
1992/04/13	01:20:03.1	51.14°N 6.05°E	6.0	15	9.2×10^{16}	Braunmiller *et al.* (1994)	9.3×10^{16}
1995/06/20	01:54:57.5	50.57°N 4.82°E	4.6	10			9.0×10^{14}
1997/10/21	16:44:39.4	48.78°N 9.72°E	4.0	10	2.3×10^{14}	Braunmiller (2002)	1.7×10^{14}
1997/11/29	20:06:09.3	50.31°N 8.35°E	4.0	7	3.0×10^{14}	Braunmiller (2002)	4.5×10^{14}
2001/06/23	01:40:05.3	50.87°N 6.17°E	4.3	10	9.23×10^{14}	www.seismo.ethz.ch/mt	5.4×10^{14}
2002/07/22	05:45:03.8	50.91°N 6.17°E	5.2	10	8.66×10^{15}	www.seismo.ethz.ch/mt	4.1×10^{15}
2003/02/22	20:41:05.5	48.35°N 6.68°E	5.7	10	1.64×10^{16}	www.seismo.ethz.ch/mt	1.5×10^{16}
2003/03/22	13:36:16.3	48.25°N 8.98°E	4.7	10	8.52×10^{14}	www.seismo.ethz.ch/mt	8.8×10^{14}
2004/05/22	05:19:03.3	50.38°N 7.44°E	4.0	10	2.78×10^{14}	www.seismo.ethz.ch/mt	1.8×10^{14}
2004/10/20	06:59:16.0	53.04°N 9.54°E	4.5	5	3.44×10^{15}	www.seismo.ethz.ch/mt	2.4×10^{15}
2004/12/05	01:52:38.8	48.12°N 8.04°E	5.1	10	8.04×10^{15}	www.seismo.ethz.ch/mt	6.8×10^{15}

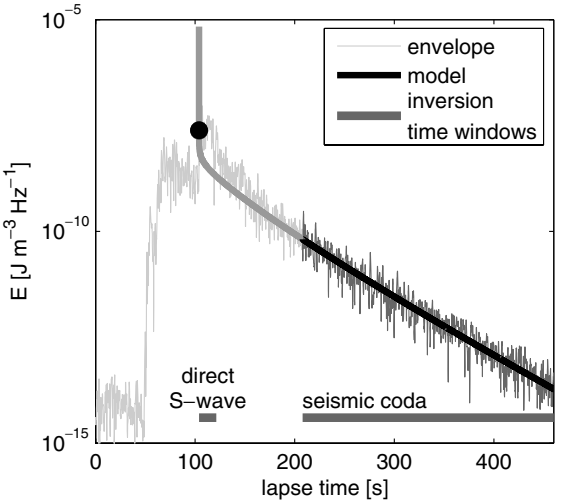

Figure 2. Example of an observed seismogram envelope (thin curve) on a logarithmic scale with the best-fitting model (bold black curve). Time windows used in the inversion are indicated at the bottom of the figure. Note that in the time window of the direct *S*-wave only the average values (black dot) of envelope and model are fitted.

(ii) We equate $E_{\rm obs}$ (eq. 6) and $E_{\rm mod}$ (eq. 5) and rearrange terms like

$$\ln\left(\frac{E_{\rm obs}(t_j, r_i)}{G(t_j, r_i)}\right) = \ln(2WR_i) - bt_j. \quad (8)$$

Here ln denotes the base *e* logarithm. By fitting a linear curve to the left-hand side of eq. (8) as function of time we obtain the appropriate values of b and (WR_i). To reduce the effect of direct surface waves and anisotropic scattering we only fit the graph in the 'coda' time window (Fig. 2) starting at twice the *S*-wave traveltime. Additionally we apply the constraint that average values of the modelled and observed envelopes within the 'direct *S*-wave' time window (Fig. 2) are equal. At distance r from the source this time window contains the samples with lapse time t in the range $3.5\,{\rm km\,s^{-1}} > r/t > 3.0\,{\rm km\,s^{-1}}$. We apply this constraint to resolve the trade-off between g_0 and (WR_i) that exists in the later coda.

(iii) With the values of b and (WR_i) obtained in step two $E_{\rm mod}$ is calculated explicitly (eq. 5) to estimate the misfit ϵ (eq. 7).

(iv) Steps one to three are repeated for a range of g_0 values. The final model for one event and one frequency band is that with the smallest value of ϵ.

(v) For the best-fitting model W and R_i are calculated explicitly by simply taking W to be the logarithmic average of all (WR_i) values. This way we assume that the average of the logarithms of the R_i is zero which means that we measure the site amplifications relative to the network mean that is assumed to be one.

The constraint that makes use of the 'direct *S*-wave' time window originates from the following problem. In a weakly scattering medium the difference between the coda of two models with different W and g_0 can be very small provided the product Wg_0 is equal for both models. The single scattering approximation (Sato & Fehler 1998, p. 47) which is valid for small g_0 predicts that the energy density $E_{\rm mod}$ is proportional to Wg_0. In this range it is inherently impossible to separate W and g_0. However, also for moderate scattering that is not adequately modelled in the single scattering approximation it can be practically impossible to separate W and g_0 due to noisy data and other simplifications in the model if only information from the coda is used.

In contrast the ballistic energy density is proportional to $We^{-(v_0 g_0 + b)t}$. Here we observe a trade-off between g_0 and b which corresponds to the known fact that intrinsic and scattering attenuation cannot be separated using unscattered energy only. However, the energy W and total attenuation can be separated because of the different time dependence.

In the inversion we fit envelopes in the 'coda' time window indicated in Fig. 2. However, we restrict the possible models to these which correctly predict the ballistic energy in the 'direct *S*-wave' time window (Fig. 2). We want to stress that in a weakly scattering medium it is on the one hand not possible to reliably estimate W form the coda alone without *a priori* knowledge of g_0. On the other hand it is impossible to estimate W solely from the ballistic wave because in order to apply radiative transfer theory which provides the source energy W we need to separate g_0 and b. We note that information from the unscattered wave is implicitly evaluated also by MLTWA to separate g_0 and b since the first time window of the MLTWA generally contains the ballistic energy.

5 RESULTS

As we simultaneously invert all available recordings we implicitly assume that there are no lateral variations in the structural parameters g_0 and b. Our results represent integral values averaged over possible regional variations. An example of the fit that we achieve with our model is given in Fig. 3. The observed envelopes are plotted as thin lines whereas bold lines represent the model envelopes. Average energy density values in the 'direct *S*-wave' time window are indicated as grey and black dots for observed and modelled envelopes, respectively. The model generally fits the envelopes in the 'coda' time window. Deviations in the 'direct *S*-wave' window are probably due to directionality of the source.

In the following sections, we will first present the results of the attenuation parameters as they are fundamental for the estimated source parameters that we present thereafter. We will also briefly mention the estimates of the site amplifications.

5.1 Attenuation parameters

Scattering strength can be expressed in terms of the total scattering coefficient g_0 which is the inverse of the mean free path or in terms of scattering attenuation parameter ${}^{Sc}Q^{-1}$. The relation between both is

$${}^{Sc}Q^{-1} = \frac{g_0 v_0}{2\pi f}, \quad (9)$$

where f denotes frequency. Fig. 4 displays g_0 as function of frequency. Small grey dots in Fig. 4 indicate measurements of individual earthquakes. The scatter of these values is due to uncertainties of the measurements but additionally regional differences of the scattering strength will increase the variations in the g_0 values. Black dots with error bars indicate the logarithmic averages of the individual measurements together with their 95 per cent confidence limits. Individual measurements range between 10^{-7} m^{-1} and 10^{-5} m^{-1}. Logarithmic averages range between 9×10^{-7} m^{-1} and 3×10^{-6} m^{-1}. There is no significant frequency dependence of g_0 and logarithmically averaged over all measurements irrespective of frequency we obtain a value of 1.45×10^{-6} m^{-1} corresponding to a mean free path of 690 km. We compare our estimates with Abubakirov & Gusev (1990), Fehler *et al.* (1992), Mayeda *et al.* (1992) and Lacombe *et al.* (2003) who studied coda waves in Kamchatka, Japan, Hawaii/Long Valley/central California and France, respectively. Table 2 summarizes the results of the different studies in frequency bands centred at 3.0 Hz. Refer to Bianco *et al.* (2002)

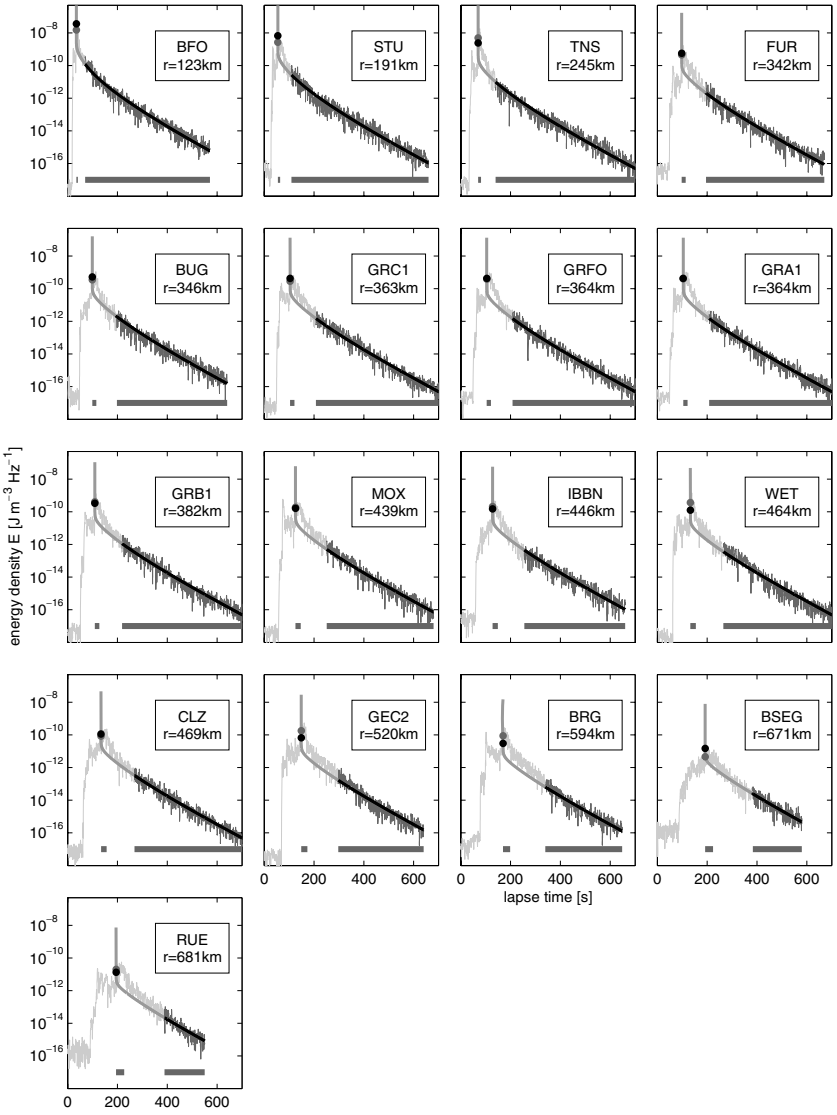

Figure 3. Comparison between the envelopes (thin curves) of the 2003-2-22 earthquake with the model (bold black curve) in the 1.5 Hz band on a logarithmic scale. Time windows used in the inversion are indicated with grey bars at the bottom of the plots. Note that in the time window of the direct *S*-wave only the average values of envelope and model are fitted. These levels are indicated as grey and black dots for envelope and model, respectively.

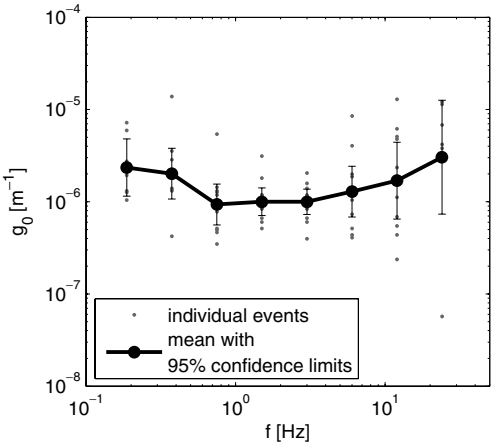

Figure 4. Results for the total scattering coefficient of *S*-waves. Grey dots: scattering coefficients measured by inversion of individual events; black dots with error bars: logarithmic mean of individual measurements with 95 per cent confidence limits.

for graphical representation of most of these results. The value obtained in the present study is low in this comparison but the difference can be attributed to geological distinctions since the central European intraplate region is likely less heterogeneous than the volcanic areas listed in Table 2. Compared to the results from France obtained by Lacombe *et al.* (2003) the difference might partially be due to a different model set-up.

The intrinsic attenuation parameter ${}^{I}Q^{-1}$ is related to the absorption parameter b as

$$ {}^{I}Q^{-1} = \frac{b}{2\pi f}. \tag{10}$$

Fig. 5 displays the results of individual measurements with small gray dots and logarithmic averages in the individual frequency bands together with 95 per cent confidence limits as black dots with error bars. Averaged over individual measurements in the separate frequency bands we obtain values of ${}^{I}Q^{-1}$ between 2.6×10^{-4} and 2.2×10^{-3}. For frequencies below 3 Hz ${}^{I}Q^{-1}$ is approximately constant at 2×10^{-3}. Above approximately 3 Hz we observe a power-law decrease like ${}^{I}Q^{-1} \propto f^{-1}$. Our values are within the range of results

Table 2. Comparison of structural parameters g_0 and Q^{-1} for different regions in frequency bands centered at 3 Hz.

Reference	g_0 in m^{-1}	${}^{I}Q^{-1}$	Region	Distance range	Model
Abubakirov & Gusev (1990)	6.7×10^{-6}	0.0032	Kamchatka	Local	half-space
Fehler *et al.* (1992)	6.5×10^{-6}	0.0026	Kanto-Tokai (Japan)	Local	half-space
Mayeda *et al.* (1992)	4.26×10^{-5}	0.00317	Long Valley	Local	half-space
	2.82×10^{-5}	0.00336	Central California	Local	half-space
	3.19×10^{-5}	0.00055	Hawaii	Local	half-space
Bianco *et al.* (2002)	2.7×10^{-6}	0.0034	Italy	Local-regional	half-space
Lacombe *et al.* (2003)	4×10^{-6}	0.0012	France	regional	layer over half-space
Abubakirov (2005)	5.3×10^{-6}	0.0031	Kamchatka	regional	half-space
this study	1.45×10^{-6}	0.0013	Germany	regional	half-space

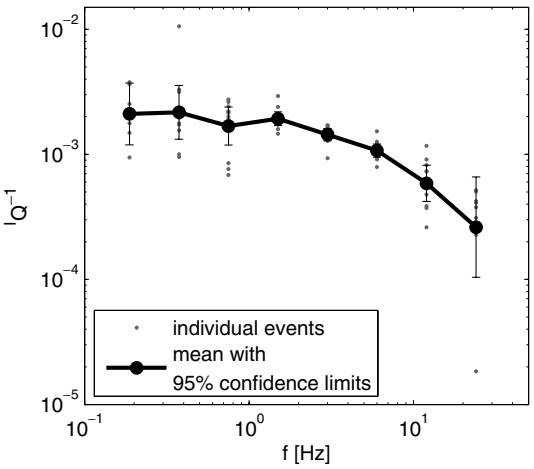

Figure 5. Results for the attenuation parameter of intrinsic absorption. Grey dots: attenuation parameter measured by inversion of individual events; black dots with error bars: logarithmic mean of individual measurements with 95 per cent confidence limits.

from different regions listed in Table 2 and very close to the results from France Lacombe *et al.* (2003). However, there may be some bias because we invert regional records with a half-space model. We probably overestimate ${}^{I}Q^{-1}$ because leakage of energy through the Moho into a weakly scattering mantle is mapped into attenuation (Margerin *et al.* 1998; Wegler 2004).

5.2 Source energy

Since our approach is on one hand based on a physical model of energy propagation and on the other hand does not require a coda normalization, our inversion parameter W can be interpreted directly. By measuring the source energy at various frequencies we obtain the source energy spectrum $W(\omega)$ of radiated S-waves. Assuming particle motion is caused by a double couple and is observed in the far field one can obtain a relation between $W(\omega)$ and the seismic moment by integrating the energy flux density over a sphere containing the source. Sato & Fehler (1998, p. 152) state

$$W(\omega) = \frac{\omega^4 |M(\omega)|^2}{10\pi\rho_0 v_0^5}, \tag{11}$$

where v_0, ρ_0 and $M(\omega)$ denote mean S-wave velocity, mean density, and the Fourier transform of the moment time function, respectively. From eq. (11) one obtains the source displacement spectrum $\omega|M(\omega)|$.

In Fig. 6 the source displacement spectra of the events listed in Table 1 are shown. Error bars correspond to the resolution of our inversion process and not to the scatter of individual measurements as in Figs 4 and 5. The misfit ϵ in eq. 7 is the variance of the logarithmic difference between the samples of the observed and modelled energy densities. We use the F-test to decide whether two models are significantly different based on the ratio of their variances ϵ. The error bars mark the range of values for the displacement spectra that can be obtained for models which cannot be distinguished from the best model according to the F-test (Buttkus 2000, p. 231) with a 5 per cent significance level.

Most of the curves show the expected characteristics of a displacement spectrum. A flat region can be observed towards the low-frequency limit whereas the displacement decays above a corner frequency. A different behaviour is found for the 2004 October event that occurred in northern Germany which is tectonically quiet. Neither low-frequency plateau nor corner frequency can be observed. We regard this as an evidence for a complex source process.

The low-frequency plateaus can be compared with seismic moments M_0^{wm} independently obtained from waveform inversions. For most of the events we use the solutions of the Swiss regional moment tensor catalogue that is available on-line at http://www.seismo.ethz.ch/mt/. Refer to Braunmiller *et al.* (2002) for examples and a description of the method. M_0^{wm} estimates for the three events before 2000 can be found in Braunmiller *et al.* (1994) and Braunmiller (2002). For the event in 1995 there is no seismic moment available. The waveform inversion estimates of M_0 are plotted as thick lines in Fig. 6. Obviously the low-frequency values of our displacement spectra match the moments from the waveform inversion well. Assuming that the corner frequencies of the events used here exceed 1.5 Hz we take the logarithmic average of the displacement spectra in the four lowest frequency bands as a coda based estimate of the seismic moment denoted M_0^{coda}. In Fig. 7 the values of seismic moment obtained in this study (M_0^{coda}) are plotted against the values from waveform modelling (M_0^{wm}). On average there is a difference of 36 per cent between the waveform and the coda results.

Another reference that is interesting to compare with the displacement spectra is the local magnitude scale. Recently Reamer & Hinzen (2004) investigated earthquakes in the northern Rhine area (around station BUG in Fig. 1) and established the relation

$$\log_{10} M_0^{Ml} = 1.083 Ml + 10.215, \tag{12}$$

between the local magnitude Ml and the seismic moment M_0^{Ml} in Nm. The superscript Ml indicates that the seismic moment M_0^{Ml} is estimated from local magnitudes. Fig. 7 also shows the comparison of M_0^{Ml} with the results from waveform modelling (M_0^{wm}). On average the difference between the magnitude- and waveform-derived moments is 57 per cent. The scatter in the magnitude-derived estimates is thus larger than that of the coda-derived estimates. However, according to the F-test with 10 degrees of freedom the difference

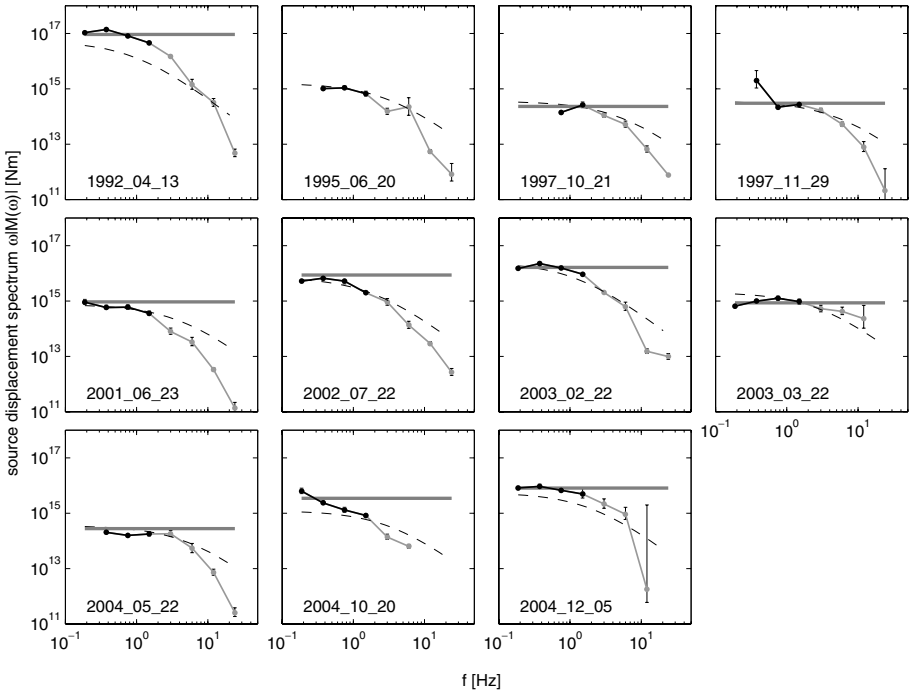

Figure 6. Double logarithmic plot of source displacement spectra of the 11 earthquakes used in this study. Numbers within the charts indicate the dates of the events in `yyyy_mm_dd` format. Dots with continuous curve: source spectra estimated in this study. Error bars correspond to 95 per cent confidence limits of the resolution of the inversion (see text for explanation). The low-frequency part shown in black is averaged to obtain M_0^{coda}. Thick horizontal line: seismic moment M_0^{wm} estimated independently using waveform modelling techniques (Braunmiller *et al.* 2002). Thin dashed curve: omega-square spectra independently calculated from local magnitudes using empirical relations. Low-frequency limit corresponds to M_0^{Ml}.

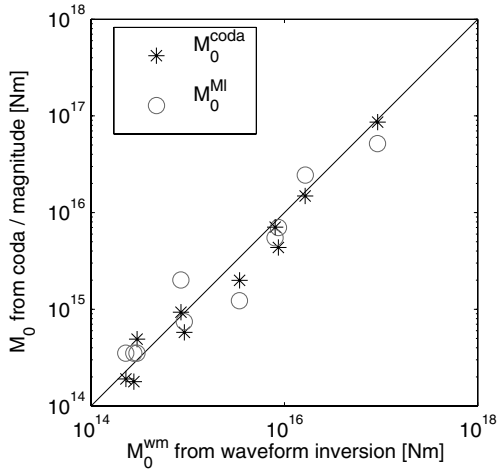

Figure 7. Scatter plot of the seismic moments obtained from seismic coda (M_0^{coda}) in this study and moments estimated from local magnitudes (M_0^{Ml}) against estimates of seismic moments from long period waveform modelling (M_0^{wm}). Straight line indicates the locations of perfect agreement of the different estimates.

between this 57 and the 36 per cent mean deviation of the coda-derived moment is not significant at a 95 per cent confidence level. This means our coda-derived estimates of the seismic moment are at least as good as the estimates that can be obtained directly from the local magnitudes.

Assuming an omega-square source model according to $\omega|M^{Ml}(\omega)| = M_0^{Ml}/(1 + f/f_c)^2$ (Aki & Richards 1980, p. 823) one can use eq. (12) to calculate an approximate source displacement spectrum if the corner frequency f_c is known. Further assuming a stress drop σ of 10 MPa, it can be obtained from $f_c = \sqrt[3]{\sigma/M_0^{Ml}} \cdot 0.49 v_0$ (Hough *et al.* 2000). This approximate source spectrum is plotted as thin dashed line in Fig. 6. Note that these approximate source spectra are solely based on the local magnitude estimated by the SZGRF.

Fig. 6 shows that also the local magnitudes can give reasonable estimates of the seismic moment. There are some differences between the magnitude- and coda-derived spectra in the corner frequency and in the high-frequency asymptote. $\omega|M^{\mathrm{coda}}(\omega)|$ shows a steeper decline than the omega-square model.

5.3 Site response

Site amplification factors for velocity amplitudes range between 0.3 and 3. Mostly they can easily be related to local geology (Table A1). In the 0.375 Hz band for example we find amplifications of crystalline sites only below 1 (logarithmic mean: 0.8) whereas stations on sediments show amplifications exclusively above 2 (logarithmic mean: 3.0). Sites on sedimentary rocks occupy an intermediate range between 0.75 and 1.75 (logarithmic mean: 1.1). As examples we show the site factors for the stations BUG and FUR in Fig. 8. BUG is situated on a clastic sedimentary rock. The site amplification is not frequency dependent with a mean of 0.9. In contrast FUR is placed on moraine over molasse (i.e. sediments). Here we see a clear amplification of a factor greater than 2. Response factors for all stations and frequencies are listed in the appendix, together with information about geology.

6 DISCUSSION

The model used in the present study is a first-order approximation of *S*-wave scattering in the earth. We neglect anisotropic scattering

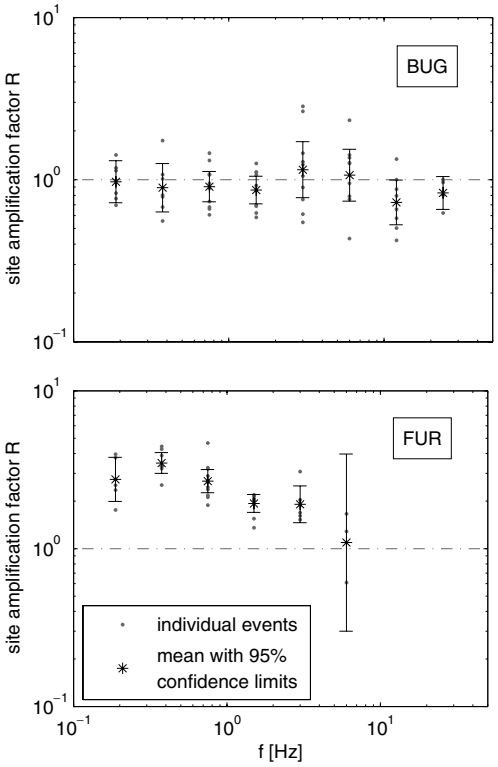

Figure 8. Site response spectra for the stations BUG and FUR. BUG is placed on sedimentary rock whereas FUR is situated on sediments.

and mode conversions, do not pay attention to source radiation patterns and assume a statistically homogeneous half-space. Some of these effects could be incorporated into our model by solving the radiative transfer equation with Monte Carlo techniques. This allows to take into account anisotropic scattering or mode conversion of elastic waves (Przybilla *et al.* 2006) . Even anisotropic sources and deterministic earth structure, like a depth-dependent velocity and scattering coefficient can be simulated (Margerin *et al.* 1998) . The improvement of the model that can be achieved by incorporating these effects will be variable and the successful application of more complex models requires detailed knowledge about the medium and the source (Hoshiba *et al.* 2001). The source radiation patterns for example will probably have a minor effect on our results because in the late coda the effect vanishes due to the averaging by multiple scattering and the direct *S*-wave is measured and averaged over a lot of stations. Note that *S*-waves always have less pronounced radiation patterns than *P*-waves irrespective of the station configuration (Sato & Fehler 1998, p.150).

The acoustic approximation is justified here because the different magnitude of the conversion scattering coefficients for *S*-to-*P* and *P*-to-*S* conversion (Aki 1992) leads to a stable partitioning of energy at large lapse times which is dominated by *S*-waves. In this regime *P*-waves carry only about 10 per cent of total energy (Ryzhik *et al.* 1996, eq. 5.40). In order to model the early *S*- and *P*-wave coda the treatment of the elastic scattering problem seems to be the most promising modification to our approach. The computational effort, however, would be substantially higher. A still unsolved problem is the treatment of conversion and scattering of surface modes.

One consequence of the half-space model is the inability to handle L_g waves. Lacombe *et al.* (2003) model L_g waves using a Monte Carlo technique to separate intrinsic absorption and scattering attenuation. Interestingly Lacombe *et al.* (2003) could not satisfactorily separate elastic and anelastic attenuation without the use of information from direct waves incorporated as total attenuation. This directly corresponds to our observation that led to the constraint of the inversion with the ballistic energy.

Nevertheless, our final results are encouraging. Though we use a very simple model we can directly relate the shape and amplitude of seismogram envelopes to the moment of the source. These moment estimates are in good agreement with independent results from moment tensor inversions. We find reasonable values for the total scattering coefficient g_0 and the intrinsic attenuation parameter ${}^{I}Q^{-1}$ and obtain site response factors that reflect local geology. We think that the approximations are justified in order to obtain fast estimates of relevant parameters without *a priori* knowledge about medium or source.

There are some technical parameters in the algorithm that might influence our results. First, the choice of the misfit function might have an effect. We verified that $\log(E_{\rm obs}/E_{\rm mod})$ is approximately Gaussian distributed in the coda time window if the model fits well. For comparison we inverted the data set using different misfit functions including the L1-norm and found no significant differences.

Another influence might come from the choice of the inversion time windows. The 'seismic coda' time window starts at two times the *S*-wave traveltime. In this part of the seismogram the distribution of energy is traditionally believed to be close to the diffusion limit (Rautian & Khalturin 1978; Wu & Aki 1985). This is not required in our method but also the assumption of isotropic scattering is a better approximation in the later coda. Additionally we exclude direct surface waves by fitting only the late coda. The 'direct *S*-wave' time window starts at the arrival of the direct *S*-wave ($v = 3.5$ km s^{-1}) and lasts until waves with apparent velocities above 3.0 km s^{-1} have passed the station. This is somewhat arbitrary but the objective was to collect energy that was radiated as *S*-wave from the source in the direction of the receiver. Taking into account finite source duration and envelope broadening due to forward scattering (Sato 1989; Saito *et al.* 2002) this appeared to be a reasonable choice. By comparing the results with inversions done with different lengths of the 'direct *S*-wave' time window we verified that the influence is small compared to the uncertainties of our estimates.

A new aspect of this method is the frequency range used for inversion. Typically only frequencies above 1 Hz have been used in studies of seismic scattering (Fehler *et al.* 1992; Mayeda *et al.* 1992; Bianco *et al.* 2002; Lacombe *et al.* 2003). On one hand this is due to the short period data used in these studies. On the other hand low-frequency coda is believed to be influenced by surface waves (Wu & Aki 1985; Abubakirov & Gusev 1990). We think that the latter argument is not well founded. Mode conversions between body and surface waves as well as surface-to-surface wave scattering are not bound to frequencies below 1 Hz. Since it is important for our purpose of estimating the low-frequency level of the source spectrum, that is, the seismic moment of the earthquakes, we further exploited the broad-band data to obtain data below the corner frequencies.

The major advantage of our method is that we can easily obtain source parameters like the seismic moment without *a priori* knowledge about attenuation functions that are needed for magnitude estimations and without waveform modelled reference events that are needed if envelopes are approximated on the basis of empirical formulae. Our approach is thus optimally suited for source parameter estimation with temporal seismic networks.

Another possible application is related to the stability of the coda compared to direct waves. If the medium parameters g_0 and ${}^{I}Q^{-1}$ and the site response factors R_i have been estimated once in a study like the present, the seismic coda can be used to obtain magnitude

estimates that are more stable than estimates from direct waves because the coda is less sensitive to source radiation patterns. In fact Mayeda *et al.* (2003) showed that coda amplitudes have three to five times less interstation scatter as compared to direct phases. Just like the method of Mayeda *et al.* (2003) our approach can be used to significantly improve the magnitude estimates in permanent seismic networks.

Compared to waveform modelling techniques our method has a fundamental advantage for the estimation of the seismic moment. Modelling waveforms requires knowledge about the Green's function of the propagation medium. Due to small-scale heterogeneities in realistic earth models this is impossible for high frequencies. Therefore, waveform techniques cannot be applied to small ($Ml <$ 3.5) earthquakes. As we model energy densities rather than waveforms our approach only requires knowledge of the energy density Green's function. In this case the phase relation between waves that interacted with these small-scale structures can be neglected and it is possible to obtain the Green's function in a statistical sense. It is thus possible with our method to obtain estimates of the seismic moment for small events with high-frequency sources.

7 CONCLUSIONS

We present a new method to extract information from the seismic coda using radiative transfer theory. It is based on the modelling of coda envelopes as *S*-waves that were isotropically scattered at randomly distributed heterogeneities in a statistically homogeneous half-space. We do not apply coda normalization but instead incorporate the effects of different sources and site responses into the inversion scheme which enables us to explicitly resolve these parameters together with medium parameters.

We can thus directly obtain source spectra and seismic moments from seismogram envelopes and we show that there is excellent agreement between our estimates and values independently obtained in moment tensor inversions. Additionally, we obtain site response factors and separate intrinsic and scattering attenuation.

ACKNOWLEDGMENTS

We like to thank the German Central Seismological Observatory (SZGRF) for easy access to the data and the Deutsche Forschungsgemeinschaft for financial support through project grant WE 2713/1-1. The helpful comments of two anonymous reviewers are greatly appreciated.

REFERENCES

Abubakirov, I.R., 2005. Attenuation characteristics of transverse waves in the lithoshere of Kamchatka estiamted from observations at the Petropavlovsk digital broadband station, *Izvestiya, Physics of the Solid Earth,* **41**(10) 813–824.

Abubakirov, I.R. & Gusev, A.A., 1990. Estimation of scattering properties of the lithosphere of Kamchatka based on Monte-Carlo simulation of record envelope of a near earthquake, *Phys. Earth planet. Int.,* **64**(1), 52–67.

Aki, K., 1980. Attenuation of shear-waves in the lithosphere for frequencies from 0.05 to 25 Hz, *Phys. Earth planet. Inter.,* **21**(1), 50–60.

Aki, K., 1992. Scattering conversions P to S versus S to P, *Bull. seism. Soc. Am.,* **82**(4), 1969–1972.

Aki, K. & Chouet, B., 1975. Origin of coda waves: source, attenuation, and scattering effects, *J. geophys. Res.,* **80**(23), 3322–3342.

Aki, K. & Richards, P.G., 1980. *Quantitative Seismology, Theory and Methods*, volume II. W. H. Freeman and Company, San Francisco, CA.

Bianco, F., Del Pezzo, E., Castellano, M., Ibanez, J. & Di Luccio, F., 2002. Separation of intrinsic and scattering seismic attenuation in the Southern Apennine zone, Italy, *Geophys. J. Int.,* **150,** 10–22.

Braunmiller, J., 2002. Moment tensor solutions of stronger earthquakes in Germany with GRSN data, in *Ten Years of German Regional Seismic Network (GRSN)*, pp. 227–235, ed. Korn, M., number Report 25, Senate Commisson for Geoscience of the Deutsche Forschungsgemeinschaft.

Braunmiller, J., Dahm, T. & Bonjer, K.P., 1994. Source mechanism of the 1992 Roermond earthquake from surface wave inversion of regional data, *Geophys. J. Int.,* **116,** 663–672.

Braunmiller, J., Kradolfer, U., Baer, M. & Giardini, D., 2002. Regional moment tensor determination in the European-Mediterranean area—initial results, *Tectonophysics,* **356,** 5–22.

Buttkus, B., 2002. *Spectral Analysis and Filter Theory in Applied Geophysics*. Springer-Verlag Berlin, Heidelberg.

Dewberry, S.R. & Crosson, R.S., 1995. Source scaling and moment estimation for the Pacific northwest network using S-coda amplitudes, *Bull. seism. Soc. Am.,* **85**(5), 1309–1326.

Fehler, M., Hoshiba, M., Sato, H. & Obara, K., 1992. Separation of scattering and intrinsic attenuation for the Kanto-Tokai region, Japan, using measurements of S-wave energy versus hypocentral distance, *Geophys. J. Int.,* **108**(3), 787–800.

Hoshiba, M., Rietbrock, A., Scherbaum, F., Nakahara, H. & Haberland, C., 2001. Scattering attenuation and intrinsic absorption using uniform and depth dependent model—application to full seismogram envelope recorded in northern Chile, *J. Seismology,* **5**(2), 157–179.

Hoshiba, M., Sato, H. & Fehler, M., 1991. Numerical basis of the separation of scattring and intrinsic absorption from full seismogram envelope—a Monte-Carlo simulation of multiple isotropic scattering, *Pa. Meteorol. Geophys., Meteorol. Res. Inst.,* **42,** 65–91.

Hough, S.E., Dollar, R.S. & Johnson, P., 2000. The 1998 earthquake sequence south of Long Valley caldera, California: hints of magmatic involvement, *Bull. seism. Soc. Am.,* **90**(3), 752–763.

Korn, M., (ed.), 2002. *Ten Years of German Regional Seismic Network (GRSN)*, Number Report 25. Senate Commisson for Geoscience of the Deutsche Forschungsgemeinschaft.

Lacombe, C., Campillo, M., Paul, A. & Margerin, L., 2003. Separation of intrinsic absorption and scattering attenuation from Lg coda decay in central France using acoustic radiative transfer theory, *Geophys. J. Int.,* **154**(2), 417–425.

Margerin, L., Campillo, M. & Van Tiggelen, B.A., 1998. Radiative transfer and diffusion of waves in a layered medium: new insight into coda Q, *Geophys. J. Int.,* **134,** 596–612.

Mayeda, K., Hofstetter, A., O'Boyle, J.L. & Walter, W.R., 2003. Stable and transportable regional magnitudes based on coda-derived moment-rate spectra, *Bull. seism. Soc. Am.,* **93**(1), 224–239.

Mayeda, K., Koyanagi, S., Hoshiba, M., Aki, K. & Zeng, Y., 1992. A comparative study of scattering, intrinsic, and coda Q^{-1} for Hawaii, Long Valley Caldera, and central California between 1.5 and 15.0 hz, *J. geophys. Res.,* **97**(B5), 6643–6659.

Mayeda, K. & Walter, W.R., 1996. Moment, energy, stress drop, and source spectra of western United States earthquakes from regional coda envelopes, *J. geophys. Res.,* **101**(B5), 11 195–11 208.

Morasca, P., Mayeda, K., Malagnini, L. & Walter, W.R., 2005. Coda-derived source spectra, moment magnitudes and energy-moment scaling in the western Alps, *Geophys. J. Int.,* **160,** 263–275.

Nakahara, H., Nishimura, T., Sato, H. & Ohtake, M., 1998. Seismogram envelope inversion for the spatial distribution of high-frequency energy radiation from the earthquake fault: application to the 1994 far east off Sanriku earthquake, Japan, *J. geophys. Res.,* **103**(B1), 855–867.

Paasschens, J.C.J., 1997. Solution of the time-dependent Boltzmann equation, *Phys. Rev. E,* **56**(1), 1135–1141.

Przybilla, J., Korn, M. & Wegler, U., 2006. Radiative transfer of elastic waves versus finite difference simulations in two-dimensional random media, *J. geophys. Res.,* **111,** B04305, doi: 10.1029/2005JB003952.

Rautian, T.G. & Khalturin, V.I., 1978. The use of the coda for determination of the earthquake source spectrum, *Bull. seism. Soc. Am.,* **68**(4), 923–948.

Reamer, S.K. & Hinzen, K.-G., 2004. An earthquake catalog for the Northern Rhine area, Central Europe (1975–2002), *Seism. Res. Lett.,* **75**(6), 713–725.

Ryzhik, L., Papanicolaou, G. & Keller, J.B., 1996. Transport equations for elastic and other waves in random media, *Wave Motion,* **24,** 327–370.

Saito, T., Sato, H. & Ohtake, M., 2002. Envelope broadening of spherically outgoing waves in three-dimensional random media having power-law spectra, *J. geophys. Res.,* **107**(B5), 3-1-3-16, doi:10.1029/2001JB000264.

Sato, H., 1989. Broadening of seismogram envelopes in the randomly inhomogeneous lithosphere based on the parabolic approximation: southeastern Honshu, Japan, *J. geophys. Res.,* **94**(B12), 17 735–17 747.

Sato, H. & Fehler, M.C., 1998. *Seismic Wave Propagation and Scattering in the Heterogeneous Earth*, Springer-Verlag, New York.

Sato, H., Nakahara, H. & Ohtake, M., 1997. Synthesis of scattered energy density for non-spherical radiation from a point shear dislocation source based on the radiative transfer theory, *Phys. Earth planet. Inter.,* **104,** 1–13.

Wegler, U., 2004. diffusion of seismic waves in a thick layer: theory and application to Vesuvius volcano, *J. geophys. Res.,* **109**(B7), doi:10.1029/2004JB003048.

Wegler, U., Korn, M. & Przybilla, J., 2006. Modelling full seismogram envelopes using radiative transfer theory with Born scattering coefficients, *Pure appl. Geophys.,* **163,** 503–531.

Wu, R. & Aki, K., 1985. The fractal nature of the inhomogeneities in the lithosphere evidenced from seismic wave scattering, *Pure appl. Geophys.,* **123**(6), 805–818.

Zeng, Y., Su, F. & Aki, K., 1991. Scattering wave energy propagation in a random isotropic scattering medium: 1. Theory, *J. geophys. Res.,* **96**(B1), 607–619.

APPENDIX: SITE RESPONSE FACTORS

Table A1. Site response factors of the 25 seismic stations that were used in this study. The '÷' sign denotes the *logarithmic* uncertainty. The site factor is to be multiplied or divided by the uncertainty to obtain the limits of the 95 per cent confidence interval. If no uncertainty is given only a single event could be inverted. The two stations marked with * are placed several 100 m below surface.

Station	Geology	0.1875 Hz	0.375 Hz	0.75 Hz	1.5 Hz	3.0 Hz	6.0 Hz	12.0 Hz	24.0 Hz
BFO	Granite	0.71 ÷ 1.61	0.76 ÷ 1.26	0.72 ÷ 1.16	0.73 ÷ 1.20	0.64 ÷ 1.28	0.57 ÷ 1.18	0.94 ÷ 1.54	1.06 ÷ 2.85
BRNL	Cenozoic sediments	3.78	4.61	3.72 ÷ 7.52	2.03				
BRG	Slate	1.10 ÷ 2.09	0.81 ÷ 1.46	0.56 ÷ 1.15	0.60 ÷ 1.16	0.90 ÷ 1.23	1.21 ÷ 8.32		
BSEG	Anhydrit	2.11 ÷ 1.19	1.23 ÷ 2.04	0.58 ÷ 1.52	0.62 ÷ 2.05	1.13	0.53		
BUG	Sedimentary rocks	0.87 ÷ 1.37	0.96 ÷ 1.41	0.88 ÷ 1.25	0.86 ÷ 1.21	1.08 ÷ 1.39	1.11 ÷ 1.42	0.72 ÷ 1.39	0.85 ÷ 1.31
CLL	Greywacke rocks	1.12 ÷ 2.18	0.91 ÷ 1.27	0.74 ÷ 1.17	1.10 ÷ 1.21	1.20 ÷ 1.23	1.85 ÷ 1.40		
CLZ	Sedimentary rocks	0.87 ÷ 1.20	0.86 ÷ 1.22	0.91 ÷ 1.13	0.84 ÷ 1.09	0.91 ÷ 1.12	1.37 ÷ 1.12	2.13 ÷ 1.37	
FUR	Moraine over Molasse	2.80 ÷ 1.37	3.45 ÷ 1.14	2.49 ÷ 1.11	1.89 ÷ 1.14	1.89 ÷ 1.34	1.06 ÷ 2.99		
GEC2	Granite	1.11 ÷ 1.27	0.77 ÷ 1.17	0.65 ÷ 1.20	0.68 ÷ 1.13	0.75 ÷ 1.45	1.30 ÷ 1.57		
GRA1	Limestone	1.28 ÷ 1.18	1.58 ÷ 1.24	1.69 ÷ 1.08	1.26 ÷ 1.09	0.98 ÷ 1.11	0.63 ÷ 1.24		
GRB1	Limestone	1.04 ÷ 1.19	1.32 ÷ 1.17	1.61 ÷ 1.09	1.73 ÷ 1.11	2.97 ÷ 1.18	2.51 ÷ 1.23		
GRC1	Limestone	0.97 ÷ 1.33	0.86 ÷ 1.22	0.97 ÷ 1.10	1.18 ÷ 1.16	0.79 ÷ 1.14	0.79 ÷ 1.50		
GRFO	Limestone	1.31 ÷ 1.17	1.57 ÷ 1.24	1.55 ÷ 1.08	1.00 ÷ 1.07	0.51 ÷ 1.06	0.63 ÷ 1.20		
GSH	Slate		0.28	0.97	0.71	0.97	1.43	1.77	1.00
HAM	Cenozoic sediments	7.26	5.03 ÷ 43.31	2.52 ÷ 8.11	1.40	1.46			
HLG	Sandstone	1.87 ÷ 3.51	1.37 ÷ 92.54	1.54 ÷ 2.35	1.68 ÷ 1.81	1.15 ÷ 10.82	1.44		
IBBN		1.21 ÷ 1.32	1.23 ÷ 1.60	1.17 ÷ 1.37	1.02 ÷ 1.26	1.22 ÷ 1.42	1.60 ÷ 1.23	2.40	
MOX	Slate	0.98 ÷ 1.35	0.87 ÷ 1.19	0.65 ÷ 1.09	0.69 ÷ 1.07	0.78 ÷ 1.08	0.94 ÷ 1.19	1.39 ÷ 4.65	
NRDL	Zechstein sediments*	1.16	1.74	0.61	0.36	0.29	0.29		
RGN	Soft sediments	2.52 ÷ 5.06	2.60 ÷ 1.94	2.23 ÷ 2.61	5.14	5.83			
RUE	Limestone	1.83 ÷ 1.53	1.16 ÷ 1.52	0.93 ÷ 1.31	0.81 ÷ 1.61				
STU	Hard marls	0.92 ÷ 1.38	0.86 ÷ 1.27	1.05 ÷ 1.20	1.82 ÷ 1.14	1.47 ÷ 1.24	0.56 ÷ 2.70		
TNS	Quartzite	0.88 ÷ 2.00	0.70 ÷ 1.42	0.72 ÷ 1.28	1.09 ÷ 1.41	0.79 ÷ 1.36	0.74 ÷ 1.65	0.79 ÷ 1.77	1.11 ÷ 1.48
UBBA	Zechstein sediments*	0.90 ÷ 17.77	0.76 ÷ 1.00	0.40 ÷ 1.76	0.40 ÷ 2.24	0.40 ÷ 1.33	0.42		
WET	Gneiss	0.89 ÷ 1.68	0.69 ÷ 1.17	0.54 ÷ 1.10	0.63 ÷ 1.17	0.78 ÷ 1.17	1.54 ÷ 1.18	2.16	2.09